Металлофиз. новейшие технол. / Metallofiz. Noveishie Tekhnol.
2015, т. 37, № 8, сс. 1063–1075
Оттиски доступны непосредственно от издателя
Фотокопирование разрешено только
в соответствии с лицензией

СТРОЕНИЕ И СВОЙСТВА НАНОРАЗМЕРНЫХ И МЕЗОСКОПИЧЕСКИХ МАТЕРИАЛОВ

PACS numbers: 61.43.Gt, 71.20.Ps, 71.23.-k, 73.20.At, 78.70.En, 81.20.Wk, 82.80.Ej

Effect of Mechanical Activation of Highly Disperse SiO_2/α-Fe_2O_3 Mixtures on Distribution of Valence Electrons

Ya. V. Zaulychnyy, V. M. Gun'ko*, Yu. V. Yavorskyi, V. I. Zarko*, S. S. Piotrowska**, and V. M. Mishchenko*

National Technical University of Ukraine 'Kyiv Polytechnic Institute', Physical Engineering Faculty, 35 Politekhnichna Str., 03056 Kyiv, Ukraine
**O. O. Chuiko Institute of Surface Chemistry, N.A.S. of Ukraine, 17 General Naumov Str., 03164 Kyiv, Ukraine*
***I. M. Frantsevich Institute for Problems of Materials Science, N.A.S. of Ukraine, 3 Krzhizhanovsky Str., 03680 Kyiv-142, Ukraine*

The crystal and electronic structures of SiO_2/α-Fe_2O_3 mixtures are analysed using X-ray diffraction and ultra-soft X-ray emission spectroscopy. The energy redistributions of the Fe*spd*, Si*sp*, and O*p* valence electrons due to changes in the mass ratio (20/80, 50/50, 80/20) of SiO_2 and α-Fe_2O_3 in the mixtures are studied. The ultra-soft FeL_α, SiL_α, and OK_α X-ray emission spectra of SiO_2/α-Fe_2O_3 mixtures are compared with those of individual iron oxide and silica powders. Interatomic interactions of surface atoms of adjacent particles occur owing to high local pressures and temperatures under mechanical treatment of the composition. Electrons' transfer from silicon cations to oxygen anions is observed as a result of the mechanical activation of SiO_2/α-Fe_2O_3 mixtures.

Енергетичний перерозподіл Fe*spd*-, Si*sp*- та O*p*-валентних електронів через зміну масового співвідношення (20/80, 50/50, 80/20) вхідних прекурсорів SiO_2 та α-Fe_2O_3 у сумішах досліджували, порівнюючи одержані від них Рентґенівські емісійні спектри FeL_α-, SiL_α- та OK_α-смуг із спектрами порошкового, чистого оксиду заліза та чистого діоксиду кремнію. Аналіза спектрів показала, що міжатомова взаємодія між поверхневими атомами відбувається внаслідок високих локальних тисків і температур при нашаруванні наночастинок діоксиду кремнію на частинки оксиду заліза. Внаслідок механоактивації відбувається перенесення електронів від катіонів

Силіцію до аніонів Оксиґену досліджуваної суміші.

Энергетическое перераспределение Fe*spd*-, Si*sp*- и O*p*-валентных электронов за счёт изменения массового соотношения (20/80, 50/50, 80/20) входных прекурсоров SiO_2 и α-Fe_2O_3 в смесях исследовали, сравнивая полученные от них рентгеновские эмиссионные спектры FeL_α-, SiL_α- и OK_α-полос со спектрами порошкового, чистого оксида железа и чистого диоксида кремния. Анализ спектров показал, что межатомное взаимодействие между поверхностными атомами происходит вследствие высоких локальных давлений и температур при наслоении наночастиц диоксида кремния на частицы оксида железа. В результате механоактивации происходит перенос электронов от катионов кремния к анионам кислорода исследуемой смеси.

Key words: hematite, nanosilica, electronic structure, ultra-soft X-ray emission spectroscopy, X-ray diffraction.

(Received March 3, 2015)

1. INTRODUCTION

Micro- and nanoparticles play an important role in various industrial processes and natural phenomena. Nanooxides and nanocomposite materials are used in photocatalysis [1], thermophotoelectric [2], as well as fillers of polymers, pigments, *etc*. These materials can be used in the fabrication of photon crystals [3] and have a highly promising potential in electrochemistry [4], as they are highly stable and nontoxic in tough conditions. Therefore, synthesis and investigation of new nanooxides and nanocomposite materials is of importance from practical point of view.

Among a variety of new materials [5–11], it is worth to mark out nanomaterials, which sorption, photocatalytic, photoelectric and electrochemical properties along with their structure–morphology characteristics are determined by the energy and charge states of atoms or ions. The energy and charge states of ions depend on energy redistribution of valence electrons of atoms of surface layers of nanoparticles with developed surface area as in nanosize SiO_2 and α-Fe_2O_3 [12–23]. Properties of such materials in nanocomposites are reciprocally supplemented [24–27]. Thus, it is important to investigate the electronic structure depending on composition of such nanomaterials and synthesis method.

One of widely used methods of processing of nanocomposite materials is mechanoactivation. Therefore, the aim of this work is to study the mechanoactivation effect on the energy distribution of the valence electrons and charge state of constituent atoms after treatment of highly disperse iron oxide and silica mixed in different ratios.

2. MATERIALS AND METHODS

2.1. Materials

Studied amorphous highly dispersed silica (HDS) had the specific surface area $S_{BET} = 300$ m^2/g (PS300) and average particle diameter $d = 9.2$ nm. Pyrogenic silica (pilot plant of the O. O. Chuiko Institute of Surface Chemistry, Kalush, Ukraine) was synthesized using $SiCl_4$ as a precursor burned in the O_2/H_2 flame resulting in hydrolysis/oxidation and formation of nanoparticles of silica.

Hematite α-Fe_2O_3 (O. O. Chuiko Institute of Surface Chemistry, Ukraine) was synthesized by thermal decomposition of hydrated iron (III) oxalate ($Fe_2(C_2O_4)_3 \cdot 5H_2O$) at 350–370°C in air. The yield of α-Fe_2O_3 is approximately 35%. Crystalline α-Fe_2O_3 had $S_{BET} = 7$ m^2/g and coherent-scattering region size $d_{CSR} = 92$ nm. This value is much smaller than the particle size determined from the specific surface area $d = 6/(S_{BET}\rho_0) = 163$ nm, where ρ_0 is the true density of hematite (5.26 g/cm^3), assuming a spherical shape of particles. This suggests that primary hematite particles are not monocrystalline.

Mechanically activated (MA) systems x-$SiO_2 + y$-Fe_2O_3 were prepared using a microbreaker (stainless steel sphere of 10 cm^3 in volume with a stainless steel ball of 0.8 cm in diameter, 30 W, and frequency 50 Hz). Treatment time was 5 minutes for all samples. Non-activated mechanical mixtures of x-$SiO_2 + y$-Fe_2O_3 were prepared by simple stirring of oxides (without strong mechanical loading) during 5 minutes and then with very short (3 s) mixing in the microbreaker. Atomic composition of SiO_2, α-Fe_2O_3 and mechanical mixtures at various mass ratios are shown in Table 1.

2.2. Methods

X-ray diffraction (XRD) investigation was carried out using a DRON-

TABLE 1. Mass and atomic composition of x-$SiO_2 + y$-Fe_2O_3 mixtures.

Mass composition	Relative contribution of atoms				
	Si	O(Si)	Fe	O(Fe)	O (total)
SiO_2	0.33333	0.66667	–	–	0.66667
Fe_2O_3	–	–	0.40000	0.60000	0.60000
$0.2SiO_2 + 0.8Fe_2O_3$	0.13307	0.26613	0.24032	0.36048	0.62661
$0.5SiO_2 + 0.5Fe_2O_3$	0.24220	0.48441	0.10935	0.16403	0.64844
$0.8SiO_2 + 0.2Fe_2O_3$	0.30467	0.60935	0.03439	0.05158	0.66093

UM1 diffractometer ('Burevestnik', St.-Petersburg, Russia) with monochromatic CuK_α-radiation. Graphite single crystal mounted on diffracted beam is used as a monochromator. The diffractograms are recorded at $2\theta = 10–90°$ with a scan step angle of 0.05° and exposure time in each point of 3–7 s. The XRD data processing is carried out using Powder Cell 2.4 program for full-contour analysis of a mixture of polycrystalline components. Analysis of diffraction maxima broadening connected with coherent-scattering region sizes (which can be considered as the average size of crystallites) and lattice strain is carried out using the Williamson–Hall method. The crystallinity is determined by normalization of integral intensity of amorphous halo in a sample to intensity of amorphous halo in completely amorphous matter.

Analysis of phase composition of samples after mechanical activation shows that phase composition of samples before and after treatment is practically the same within the experimental error range. However, the values of d_{CSR} decreased for hematite crystallites (Table 2).

X-ray emission spectra of atoms of x-$SiO_2 + y$-Fe_2O_3 were obtained using ultra-soft X-ray emission spectrometry (USXES) method [4] applying RSM-500 (SCBXA, 'Burevestnik', St.-Petersburg, Russia) X-ray spectrometer-monochromator. Energy of electron beam was $E = 5$ keV and intensity was $I = 5 \cdot 10^{17}$ electron·cm^{-2} for the OK_α and $E = 7$ keV, $I = = 5 \cdot 10^{17}$ electron·cm^{-2} for FeL_α and $E = 4$ keV, and $I = 2 \cdot 10^{17}$ electron·cm^{-2} for the SiL_α band. The excitation mode used does not lead

TABLE 2. Phase composition, coherent-scattering region size (d_{CSR}) and change of coherent-scattering region size (Δd_{CSR}) in x-$SiO_2 + y$-Fe_2O_3 samples depending on mass ratio of initial precursors.

Sample	Phase composition, %	d_{CSR}, nm	Δd_{CSR}, nm
α-Fe_2O_3	α-Fe_2O_3— ≅ 100	92	2
MA α-Fe_2O_3	α-Fe_2O_3— ≅ 100	90	
$0.2SiO_2 + 0.8Fe_2O_3$	α-Fe_2O_3— ≅ 80 Am. SiO_2— ≅ 20	94	8
MA $0.2SiO_2 + 0.8Fe_2O_3$	α-Fe_2O_3— ≅ 80 Am. SiO_2— ≅ 20	86	
$0.5SiO_2 + 0.5Fe_2O_3$	α-Fe_2O_3— ≅ 50 Am. SiO_2— ≅ 50	93	15
MA $0.5SiO_2 + 0.5Fe_2O_3$	α-Fe_2O_3— ≅ 50 Am. SiO_2— ≅ 50	78	
$0.8SiO_2 + 0.2Fe_2O_3$	α-Fe_2O_3— ≅ 20 Am. SiO_2— ≅ 80	82	22
MA $0.8SiO_2 + 0.2Fe_2O_3$	α-Fe_2O_3— ≅ 20 Am. SiO_2— ≅ 80	60	

to the formation of radiation defects in the materials.

Residual pressure in an X-ray tube and a spectrometer detector was $2.67 \cdot 10^{-4}$ N·m^{-2}. Samples were rubbed into copper anode (etched and rinsed in ethanol) cooled by running water to prevent oxygen thermodesorption and sintering of SiO_2 and α-Fe_2O_3 nanoparticles during measurements. Intensity of X-ray quanta in the energy region $h\nu$ = = 510–535 eV corresponding to OK_α band was measured to persuade in absence of overlap of CuO OK_α spectra and OK_α bands of the studied samples. The repeated measurements after sample investigation showed that intensity of quanta generated by copper anode in mentioned energy region did not exceed background intensity. The forth–eighth spectra were analysed to obtain reliable results.

Diffraction grating with groove density of 600 mm^{-1} and curvature radius of 6 m (OK_α), and 2 m (AlL_α and FeL_α) is used. In the first case, filtering mirror with gold and, in the second case, filtering mirror with polystyrene are used to screen the CK_α line. Instrumental distortions measured by comparison of theoretical and measured widths of the TiL_1 line at I_{max} at the wave length λ = 3.1nm are smaller than 0.2 eV that converting to the wave length λ = 2.36 nm, where the OK_α localizes, is 0.3 eV. X-ray photons are registered using secondary electron multiplier with primary CsJ photocathode.

3. RESULTS AND DISCUSSION

In order to analyse the effect of mechanical activation on interatomic interactions, namely on a character of electron distributions in oxygen, silicon, and iron atoms, it is necessary to determine the energy regions, where Op, Sisd, and Fesd valence electrons localize for the studied materials. The energy distributions of valence electrons in various silicas were analysed in detail elsewhere [24–26]. It is shown [24–26], that lower subband corresponds to covalent-binding states in silica, and the high-energy OK_α band describes non-binding electronic states occupied by electrons transferred from silicon to oxygen.

From comparison of the OK_α and FeL_α bands with calculations of partial density of states [27] in a common energy scale, it is clear that the OK_α band reflects mainly O2p states of oxygen strongly hybridized with Fe3d orbitals. Peculiarities of the OK_α band are observed in the same energy region as Van Hove singularities are in density of the Op and Fe3d states.

Shapes of the OK_α and FeL_α bands (Fig. 1) are similar with exception of a low-energy region, where subband 'a' appears.

This subband, which according to the calculations of the partial densities of states [27], represents high density of the Fe3d states that is three times higher than that of the Op states, and it is separated from the high-energy region by a deep minimum. Such distribution of the

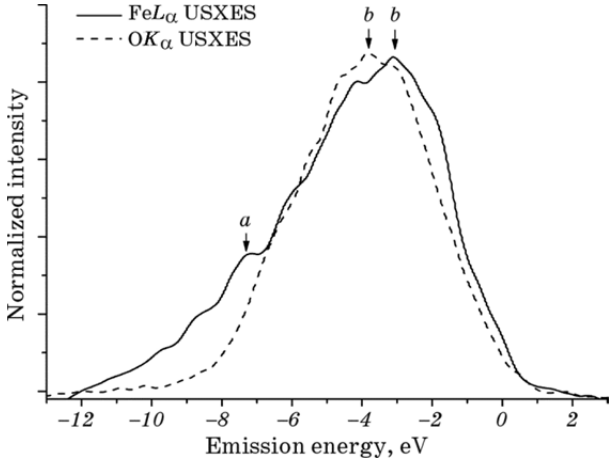

Fig. 1. The FeL_α and OK_α USXES of pure Fe_2O_3. Spectra are plotted in a common energy scale. The spectral features are labelled by *a* and *b*. All the spectra of samples have been normalized to the peak *b*.

electron states in α-Fe_2O_3 differs from that in silica. Since the shape of OK_α and FeL_α bands in the energy (−7–0) eV are very similar, it indicates that this part of the valence band hybridized strongly confirming data calculations [27], although these data by content of Fe3*d* states is lower than O*p* orbitals. This indicates the valence-binding character of the electron states in the whole valence band in contrast to that of SiO_2.

Figure 2 shows that the OK_α bands of α-Fe_2O_3 before and after me-

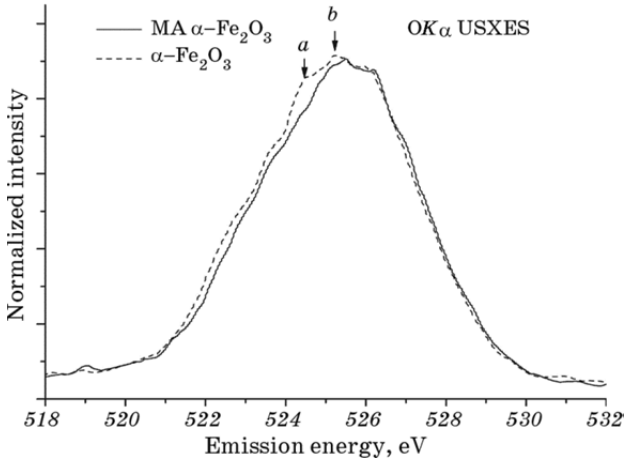

Fig. 2. The OK_α USXES of α-Fe_2O_3 and mechanically activated (MA) α-Fe_2O_3. The spectral features are labelled by *a* and *b*. All the spectra of samples have been normalized to the peak *b*.

chanical activation are almost similar with exception of narrowing of '*a*' feature in near-peak region of the OK_α of α-Fe_2O_3 after mechanical activation by 0.5 eV.

Total width of the OK_α band of α-Fe_2O_3 after mechanical activation slightly decreases due to a shift of a low-energy part of the band by 0.2 eV. It is possibly occurred due to partial dehybridization of the Fe*d* + + O*p* states when ion–covalent bonds break during nanoparticles grinding under mechanical activation (Table 2). It is confirmed by d_{CSR} decreasing.

Analysis of the OK_α bands of x-$SiO_2 + y$-Fe_2O_3 mixtures with different mass and atomic composition (Table 1) shows narrowing of OK_α bands when going from α-Fe_2O_3 to SiO_2 and sharpening *a* maximum that is typical for SiO_2 (Fig. 3). Maximum *b* shifts toward higher energy and becomes narrower in a low-energy part of the OK_α band, when maintains SiO_2 increase in the mechanical mixture. It confirms prevalent contribution of SiO_2 in a source mixture.

Narrowing OK_α band of mixture containing 20% SiO_2 by 0.3 eV in a near-peak region is caused by a shift of the long-wave contour *c* toward higher energy. Shift of the low-energy contour toward the short-wave

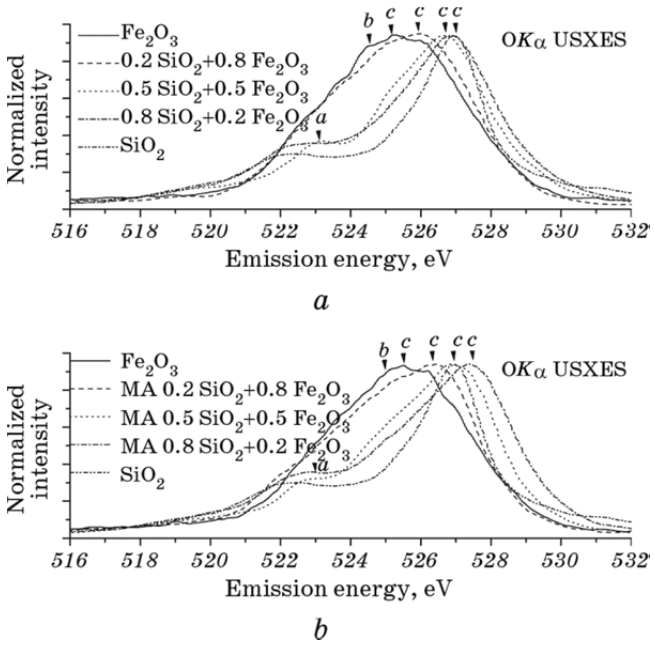

Fig. 3. The OK_α USXES of x-$SiO_2 + y$-Fe_2O_3 mixtures with different mass ratios: *a*—mechanical mixtures, *b*—mechanically activated (MA) mixtures. The spectral features are labelled by *a*, *b*, and *c*. All the spectra of samples have been normalized to the peak *c*.

TABLE 3. Dependence of differences in shifts of contours of the OK_α bands of x-SiO_2 + y-Fe_2O_3 mixtures relative to the OK_α band of Fe_2O_3 on composition before and after mechanical activation.

Mixture composition	Mechanical mixture		Mechanically activated mixture	
	ΔE of low-energy region, eV	ΔE of high-energy, eV	ΔE of low-energy region, eV	ΔE of high-energy, eV
Fe_2O_3	0	0	0.20–0.50	0
SiO_2	2.70	0.20–1.0	–	–
$0.2SiO_2 + 0.8Fe_2O_3$	0.20–0.30	0.2–0.40	0.36	0.50
$0.5SiO_2 + 0.5Fe_2O_3$	1.61	0.70	1.57	1.02
$0.8SiO_2 + 0.2Fe_2O_3$	2.07	0.90	2.09	1.46

side is 1.61 and 2.7 eV for 50 and 80% wt. of SiO_2 in the mechanical mixtures, respectively.

Maximal shift of the high-energy contour of the OK_α band toward shorter wave by 0.9 eV occurs at minimal content of Fe_2O_3 at 20% wt. When content of Fe_2O_3 increases to 50 and 80% wt., the high-energy contour of the OK_α band shifts by 0.7 and 0.3 eV, respectively. Difference in the energy positions of the high-energy contours of the OK_α bands of α-Fe_2O_3 and SiO_2 powders is 0.6 eV. Therefore, the shift of the high-energy contour of the OK_α band of mixture with 80% wt. of SiO_2 is not connected with dominant contribution of the OK_α of SiO_2.

The shift of the long-wave contours of the OK_α bands of the mechanically activated mixtures is almost similar to that of the mechanical mixtures (Table 3). The short-wave contours of the OK_α bands of the mechanically activated mixtures shift toward higher energy much greater than that for the mechanical mixtures (see Table 3). Namely, the high-energy contour of the OK_α band of the mechanically activated mixture containing 80% wt. of silica is shifted by 1.46 eV relative to that of Fe_2O_3. This value is by 0.5 eV higher than that of the mechanical mixtures.

Value of a shift of the OK_α bands decreases to 1.0 and 0.5 eV with decreasing SiO_2 content to 50 and 20% wt., respectively. Increasing intensity in the high-energy part of the OK_α bands due to mechanical activation of the mixture indicates an increase in the occupation of the 2p states of oxygen near the top of the valence band.

To explain this effect, it is necessary to compare the OK_α emission bands of the mechanical and mechanically activated mixtures. Low-energy contours of the OK_α bands of mixtures before and after activation near the bottom of the valence band are absolutely similar (Fig. 4). This testifies to absence of the effect of mechanical activation on elec-

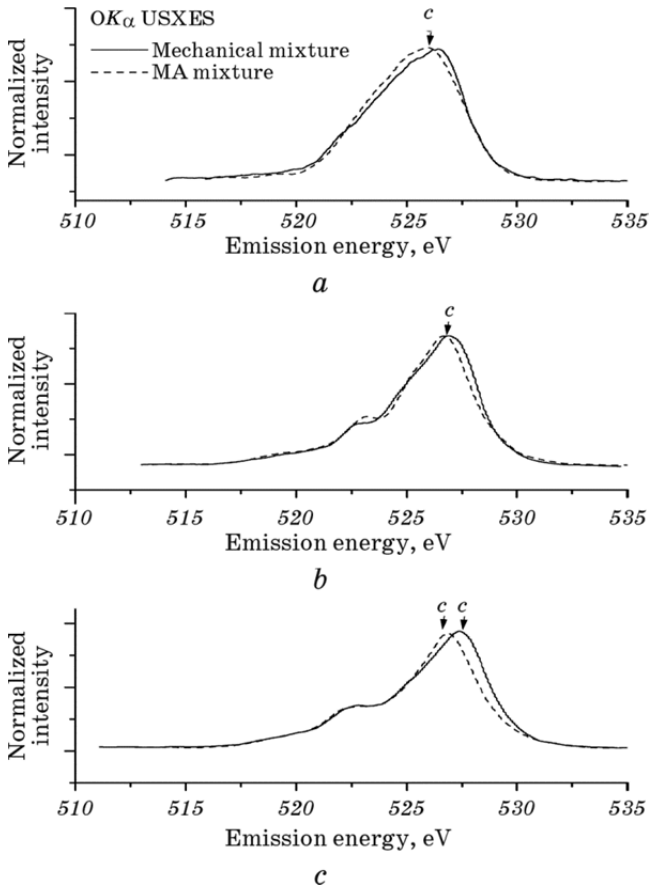

Fig. 4. The OK_α USXES of mechanical and mechanically activated (MA) mixtures: $0.2SiO_2 + 0.8Fe_2O_3$ (*a*), $0.5SiO_2 + 0.5Fe_2O_3$ (*b*), $0.8SiO_2 + 0.2Fe_2O_3$ (*c*). All the spectra of samples have been normalized to the peak *c*.

trons in deep covalent-binding states. Electrons from the energy region corresponding to photon energy $h\nu = 525.4–257.0$ eV redistribute to the energy region of 527–530 eV (Fig. 4).

Intensity of the low-energy part of the OK_α emission band decreases less if content of SiO_2 increases. Its value becomes maximal in the OK_α bands of the sample with maximal content of SiO_2.

Intensity of the SiL_α band decreased in a photon energy region $h\nu = 90.6–94.6$ eV (Fig. 5) that indicates a decrease in the occupation of the Si*sd* states in a central part of the valence band. This decrease of intensity diminishes if content of SiO_2 increases. Thus, the SiL_α bands of the mechanical and mechanically activated $0.8SiO_2 + 0.2Fe_2O_3$ samples almost coincide. The ratio of x-SiO_2 and y-Fe_2O_3 decreases in atomic percents more than in mass percents (Table 1). Therefore, contribu-

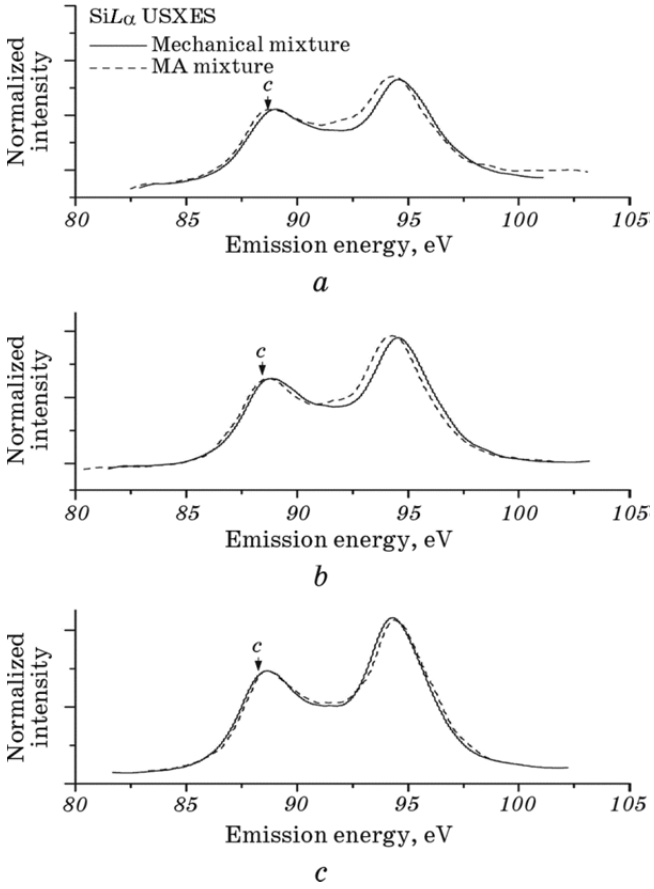

Fig. 5. The SiL_α USXES of mechanical and mechanically activated (MA) mixtures: $0.2SiO_2 + 0.8Fe_2O_3$ (*a*), $0.5SiO_2 + 0.5Fe_2O_3$ (*b*), $0.8SiO_2 + 0.2\ Fe_2O_3$ (*c*). All the spectra of samples have been normalized to the peak *c*.

tion of silicon ions into emission of the SiL_α band and oxygen ions increases, when content of α-Fe_2O_3 decreases. Supposed transfer of electrons to oxygen ions of α-Fe_2O_3 and SiO_2 did not occur due to mechanical activation, than a shape of the OK_α band had to approach to that of SiO_2. However, a shift of the high-energy contour of the OK_α band toward higher energy is maximal for a sample with the maximal content of SiO_2 due to the mechanical activation of $0.2Fe_2O_3 + 0.8SiO_2$ mixture. It indicates that electrons transfer to anions of SiO_2 and α-Fe_2O_3 is caused by the mechanical activation.

The increase in the SiO_2 content and the decrease in the relative number of α-Fe_2O_3 anions points out that transfer of charge to α-Fe_2O_3 anions increases due to the mechanical activation. As a result, intensity of the high-energy contour of the OK_α band increases with α-Fe_2O_3

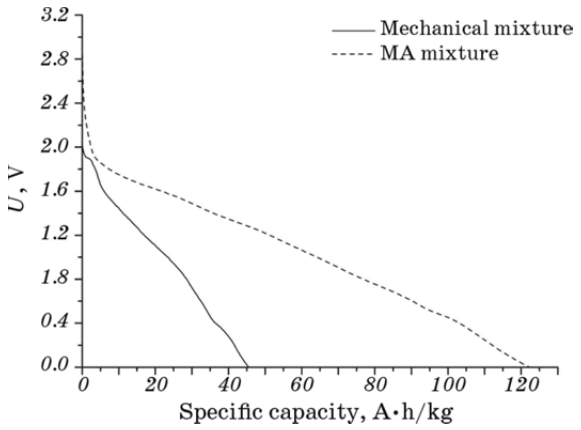

Fig. 6. Discharge curves of cells with cathode material based on mechanical and mechanically activated $0.8SiO_2 + 0.2Fe_2O_3$ mixtures.

content decreasing. It is possible, if the interatomic interactions between surface atoms of α-Fe_2O_3 and SiO_2 nanoparticles rise.

The O*p* orbitals of α-Fe_2O_3 and SiO_2 nanoparticles could overlap under high local pressures during mechanical activation. Hybridized Fe3*d* + O*p* states under the top of the valence band could be occupied. Breakage of the Si–O bonds, when SiO_2 nanoparticles are under action of larger and harder α-Fe_2O_3 particles, can cause increase of the energy of electrons in non-binding O*p* states in silica nanoparticles.

This result can explain the charge capacity of cells with cathode based on mechanical and mechanically activated $0.8SiO_2 + 0.2Fe_2O_3$ mixtures. Anode of electrochemical cell was made of lithium. Lithium hexafluorophosphate in ethyl carbonate:diethyl carbonate (1:1) $LiPF_6$ is used as an electrolyte.

Increase of occupation of O*p* states near the top of valence band due to mechanical activation results in increasing of the charge state of oxygen in tetrahedral environment of silicon. It promotes increasing of the degree of intercalation of lithium ions in the channels of structure of cathode material, resulting in increased charge capacity of electrochemical cell (Fig. 6).

Figure 6 shows that specific capacity of cell with cathode material based on mechanically activated $0.8SiO_2 + 0.2Fe_2O_3$ mixture is by 76.88 A·h/kg higher than that based on mechanical mixture. Whereas, power of cell with cathode material based on MA mixture is 2.75 times higher than that based on mechanical mixture.

4. CONCLUSIONS

The mechanical activation of the mixtures of amorphous nanosilica

particles (d_{av} = 9.2 nm in average diameter) and crystalline α-Fe_2O_3 particles (d_{CSR} = 92 nm and d_{av} = 163 nm) leads to diminution of the values of d_{CSR}. This diminution enhances with decreasing of hematite particles content. Interatomic interactions between the surface atoms of coarse α-Fe_2O_3 and finer SiO_2 nanoparticles occur due to high local pressures and temperatures under the mechanical activation of the mixtures. Electrons transfer from silicon cations to oxygen anions belonging to both α-Fe_2O_3 and SiO_2 owing to mechanical activation of x-$SiO_2 + y$-Fe_2O_3 mixtures. Increase of occupation of Op states near the top of valence band due to mechanical activation results in increasing of the charge state of oxygen in tetrahedral environment of silicon. It promotes and increases the degree of intercalation of lithium ions in the channels of structure of cathode material, resulting in increased charge capacity of electrochemical cell.

REFERENCES

1. X. X. Yu, S. W. Liu, and J. G. Yu, *Appl. Catal. B*, **104**: 12 (2011).
2. V. Rinnerbauer, S. Ndao, Y. X. Yeng, W. R. Chan, J. J. Senkevich, J. D. Joannopoulos, M. Soljačič, and I. Celanovic, *Energy Environ. Sci.*, **5**: 8815 (2012).
3. T. Ding, K. Song, K. Clays, and C. H. Tung, *Adv. Mater.*, **21**: 1936 (2009).
4. Ya. V. Zaulychnyy, Yu. M. Solonin, O. O. Foya, O. Yu. Khyzhun, and O. Vasylkiv, *Metallofiz. Noveishie Tekhnol.*, **30**, No. 2: 169 (2008).
5. R. H. French, H. Mullejans, and D. J. Jones, *J. Am. Ceram. Soc.*, **81**: 2549 (1998).
6. Sh.-D. Mo, W. Y. Ching, and R. H. French, *J. Phys. D: Appl. Phys.*, **29**: 1761 (1996).
7. Y. Matsumoto, U. Unal, N. Tanaka, Ak. Kudo, and H. Kato, *J. Solid State Chem.*, **177**: 4205 (2004).
8. E. P. Reddy, L. Davydov, and P. G. Smirniotis, *J. Phys. Chem. B*, **106**: 3394 (2002).
9. F. Gracia, J. P. Holgado, A. Caballero, and A. R. Gonzalez-Elipe, *J. Phys. Chem. B*, **108**: 17466 (2004).
10. J. L. Gole, J. D. Stout, C. Burda, Y. Lou, and X. Chen, *J. Phys. Chem. B*, **108**: 1230 (2004).
11. Ya. V. Zaulychnyj, O. O. Foya, V. M. Gun'ko, V. I. Zarko, I. F. Myronyuk, T. V. Gergel, and V. L. Chelyadyn, *Physics and Chemistry of Solid State*, **9**: 767 (2008).
12. P. Picozzi, *Solid State Commun.*, **95**: 313 (1995).
13. T. Guerlin, H. Sauer, W. Engel, and E. Zeitler, *phys. status solidi (a)*, **150**: 153 (1995).
14. F. Bart, F. Jollet, J. P. Duraud, and L. Douillard, *phys. status solidi (b)*, **176**: 163 (1993).
15. F. Bart, M. Gautier, F. Jollet, and J. P. Duraud, *Surf. Sci.*, **306**: 342 (1994).
16. B. Gilbert, B. H. Frazer, F. Naab, and J. Fournelle, *Am. Min.*, **88**: 763 (2003).
17. A. Shulakov, A. Brajko, S. Bukin, and V. Drozd, *Phys. Solid State*, **46**: 1868

(2004).
18. G. Rollmann, A. Rohrbach, P. Entel, and J. Hafner, *Phys. Rev. B*, **69**: 1651071 (2004).
19. J. O. Artman, J. C. Murphy, and S. Poner, *Phys. Rev.*, **138**: 912 (1965).
20. L. Armelaoy, M. Bettinelliz, M. Casariny, G. Granozziy, E. Tondelloy, and A. Vittadini, *J. Phys.: Condens. Matter*, **7**: 299 (1995).
21. I. S. Jacobs, R. A. Beyerlein, S. Poner, and J. P. Remeyka, *Int. J. Magnetism*, **1**: 193 (1971).
22. P. Canepa, E. Schofield, A. V. Chadwick, and M. Alfredsson, *Phys. Chem. Chem. Phys.*, **13**: 12826 (2011).
23. J.-F. Lin, J. S. Tse, E. E. Alp, J. Zhao, M. Lerche, W. Sturhahn, Y. Xiao, and P. Chow, *Phys. Rev. B*, **84**: 064424 (2011).
24. D. A. Donatti, A. Ibanez Ruiz, and D. R. Vollet, *J. Non-Cryst. Solids*, **351**: 1226 (2005).
25. V. M. Gun'ko, V. Ya. Ilkiv, Ya. V. Zaulychnyy, V. I. Zarko, E. M. Pakhlov, and M. V. Karpetz, *J. Non-Cryst. Solids*, **403**: 30 (2014).
26. B. Gilbert, B. H. Frazer, F. Naab, J. Fournelle, J. W. Valley, and G. De Stasio, *Am. Min.*, **88**: 763 (2003).
27. H. Yang, W. Mi, H. Bai, and Y. Cheng, *RSC Adv.*, **2**: 10708 (2012).